Self-Assembly of Chiral-at-End Diketopyrrolopyrroles : Symmetry Dependent Solution and Film Optical Activity and Photovoltaic Performance

By

Paul A. Hume, *[a, ǂ] James P. Monks,[a,b] Flavia Pop,[a, ∓], E. Stephen Davies,[a] Roderick C.I. MacKenzie[c] and David B. Amabilino*[a,b]

[a] School of Chemistry, University of Nottingham
University Park, NG7 2RD, UK
E-mail: david.amabilino@nottingham.ac.uk

[b] The GSK Carbon Neutral Laboratories for Sustainable Chemistry
University of Nottingham, Jubilee Campus, Triumph Road, Nottingham, NG7 2TU, UK

[c] Faculty of Engineering, University of Nottingham
University Park, NG7 2RD, UK

ǂ Present address: School of Chemical Sciences, The University of Auckland, 23 Symonds Street, Auckland, 1010, New Zealand
E-Mail: p.hume@auckland.ac.nz

∓ Present address: Laboratoire MOLTECH-Anjou, UMR 6200 CNRS
UFR Sciences, Bât. K, 2 bd. Lavoisier, 49045 Angers, France

Abstract: Chiral thiophene-diketopyrrolopyrrole derivatives have been synthesised to investigate the potential of stereochemistry and symmetry as a means of modulating properties by influencing self-assembly of these purely organic materials. In particular, derivatives of diketopyrrolopyrrole were employed because of their proven interest as dyes, especially for organic solar cells. The natural product myrtenal was used as the source of stereochemistry, introduced through a Kröhnke reaction of a thiophene-bearing pyridinium salt and diketopyrrolopyrroles were prepared through Suzuki coupling with this chiral moiety at one end only as well as at both ends. Absorption spectroscopy and electrochemistry confirmed the potential suitability of the compounds for photovoltaic devices. The nanostructures formed by the compounds have been probed with circular dichroism spectroscopy in solution and in films. It is shown that a chiral C_2 symmetric molecule assembles in solution giving a strong circular dichroic signal while as a film this optical activity is nulled, whereas an asymmetric homologue is most optically active as a thin film. The X-ray crystal structure of the asymmetric compound shows a polar order of the molecules that might explain this observation. The lack of optical activity in solution is very likely a result of the high solubility of the compound. The results reaffirm the sensitivity of circular dichroism spectroscopy to inter-chromophore organisation, whereas absorption spectroscopy in the visible region reveals only slight changes to the bands. The differing order in the compounds also affects their performance in bulk heterojunction photovoltaic devices. Atomic force microscopy of the blended thin films with the fullerene derivative usually employed ($PC_{61}BM$) showed that smooth and well mixed films were achieved, with the conditions required during spin coating depending greatly on the derivative, because of their differing solubility. The apparently better performance of the symmetrical compound (although with very low efficiency) is probably a result of the alignment of the molecules inferred by the circular dichroism experiments, whereas the asymmetric compound presumably adopts a twisted supramolecular organisation.

Introduction

While chiral materials show remarkable self-assembled nanostructures,[1,2] in the context of functional materials for organic photovoltaic devices (OPVs) the influence of symmetry and stereochemistry possessed by molecular or polymeric components does not show any consistent trends.[3-8] The degree and nature of molecular order in the active layer of OPVs is a vital factor influencing performance,[9-16] where supramolecular arrangement[17] influences morphology, exciton splitting and charge carrier mobility.[18] In contrast to other parameters, such as redox and optical characteristics, the molecular order in the active layer remains hard to control. In addition to π-π stacking of chromophores, current strategies to improve device performance targeting molecular arrangement utilise hydrogen bonding,[19-21] dipolar interactions[22] and other supramolecular approaches.[23-25] The goal of this work is to prepare small molecule chiral materials of different symmetries that have well defined structures that can be probed precisely spectroscopically, and with potential for use in OPVs. It is hoped that the lessons learned from these materials will ultimately lead to improved device performance through symmetry controlled stereoselective self-assembly.

Materials based on 1,4-diketopyrrolo[3,4-c]pyrrole (DPP, Figure 1) have gained considerable interest as active layer constituents in OPVs and organic field-effect transistors (OFETs) as a result of their high charge-carrier mobility, favourable photophysical properties, synthetic accessibility and stability.[26-29] The DPP core exhibits a high tendency to aggregate through π-π interactions and hydrogen bonding between adjacent lactam moieties.[30-33] The lactam unit is therefore commonly masked with an alkyl group, although unprotected DPP can improve device performance through increased charge mobility compared with the fully substituted compounds.[34] DPP based materials retaining solubility whilst possessing a tendency to self-assemble with a high degree of molecular order are therefore appealing. Symmettry can also play a role in this ordering.[35] We wished to explore the attachment of chiral units at the end positions of bis thiophen-2-yl-DPP.

Here we report the influence of molecular structure on self-assembly for two novel chiral-at-end diketopyrrolopyrrole dyes.

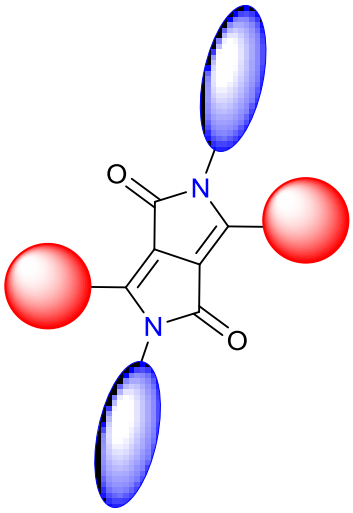

Figure 1. General chemical structure of the DPP chromophore and possible positions for chiral substituents, lateral in blue ("side" substitution) and main chain in red ("end" substitution when the stereogenic centre is at the extreme of the red symbol).

Results and Discussion

Synthesis. Compound **3** (Scheme 1), which could be covalently linked with the DPP core via cross-coupling, was chosen because of the rigidity of the aliphatic framework derived from (1*R*)-(−)-myrtenal that might minimise conformational defects in the eventual materials (more flexible chains can adopt many polymorphic conformations). In addition, the thiophene and pyridine units would extend the π-conjugation length in the molecule, decreasing the optical energy-gap. Compound **3** was constructed by Kröhnke reaction of pyridinium salt **2** (made from **1**) and (1*R*)-(−)-myrtenal.[36,37]

Conversion of **3** to bromide **4** and boronic ester **5** was achieved by *N*-bromosuccinimide bromination and Hartwig borylation, respectively.[38] Clean formation of boronate **5** was judged by analysis of the crude reaction mixture, which was engaged directly in the subsequent reaction. Suzuki cross-coupling of known dibromide **6**[39] and boronate **5** gave **7** as a blue

solid. To construct mono-coupled DPP **9**, **8** was reacted with a single equivalent of bromide **4** under CH-functionalisation conditions.[40] Although the reaction was not selective for the formation of the mono-adduct, **9** was isolated in 18% yield as a purple solid.

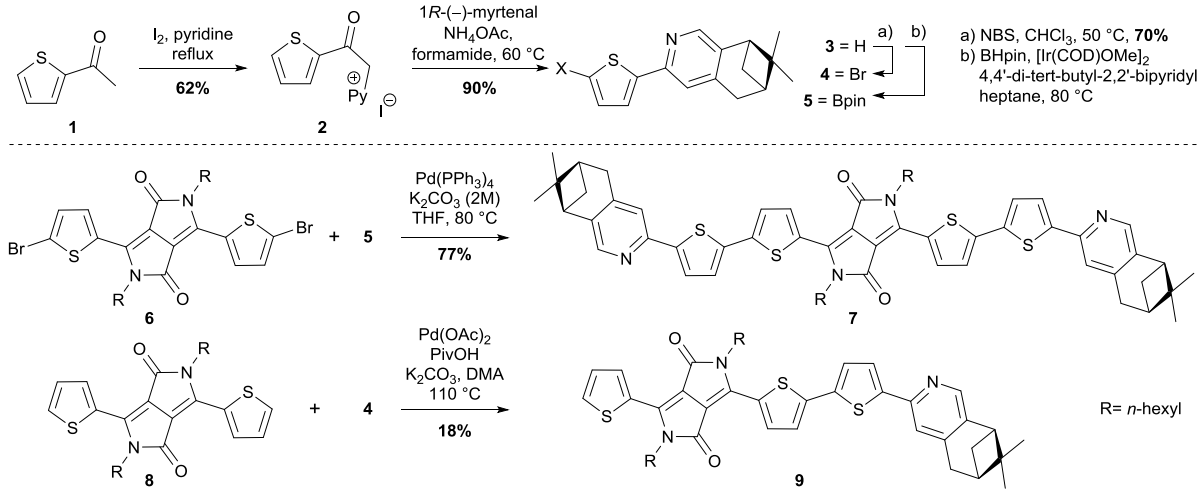

Scheme 1. Synthesis of chiral DPPs 7 and 9.

Optical Properties. The optical properties of **7** and **9** in solution were studied by UV-visible absorption and steady-state fluorescence spectroscopy (Figure 2, **8** is included for comparison and key parameters are listed in Table 1). The strengths of electronic transitions were assessed both by the extinction coefficients at the absorption maxima and by integration of the absorption band. The integrated absorption coefficients provided estimates of the square modulus of the relevant transition dipole moments $|\boldsymbol{\mu}_{ge}|^2$. The optical energy-gap (E_g) was estimated using the onset of absorption wavelength. The absorption spectra of compounds **7**, **8** and **9** show structured low energy bands, the positions of which are red shifted in line with increasing chromophore conjugation.

The absorption strength associated with the HOMO-LUMO transition also increases with conjugation. The fluorescence spectra of **7**, **8** and **9** are structured. The fluorescence quantum yield of **9** is ca. 20% and has the largest Stokes' shift of the series, indicating more significant structural differences occur between the ground and excited states. The fluorescence

quantum yield for **7** (30%) is slightly higher than that of **9** but both are significantly lower than that of **8** (ca. 60%). The thin-film absorption spectra of compounds **7** and **9** exhibited significant broadening of the absorption bands and development of a low energy shoulder (located at ~690 nm and ~650 nm for **7** and **9** respectively, see Supporting Information). Interestingly, the peak absorption for compound **9** occurs at 547 nm in the thin film, with a spectral profile reminiscent of perylene H-aggregates where the chromophores are rotationally offset with respect to one another.[41]

Table 1. Optical properties of compounds **7-9** in solution.[a]

	λ_{max} (nm)	ε_{max} [b] (M^{-1} cm^{-1})	$\lvert\mu_{ge}\rvert^2$ (D^2)	E_g [c] (eV)	λ_{em} (nm)	Φ_{fl} (%)
8	549	32900	46	2.18	676	62
9	579	49000	89	1.94	559	20
7	647	61400	129	1.81	560	30

[a] Spectra recorded as solutions in dichloromethane at 20 °C. [b] First absorption maxima. [c] Determined according to 1240/ λ(onset) (nm).

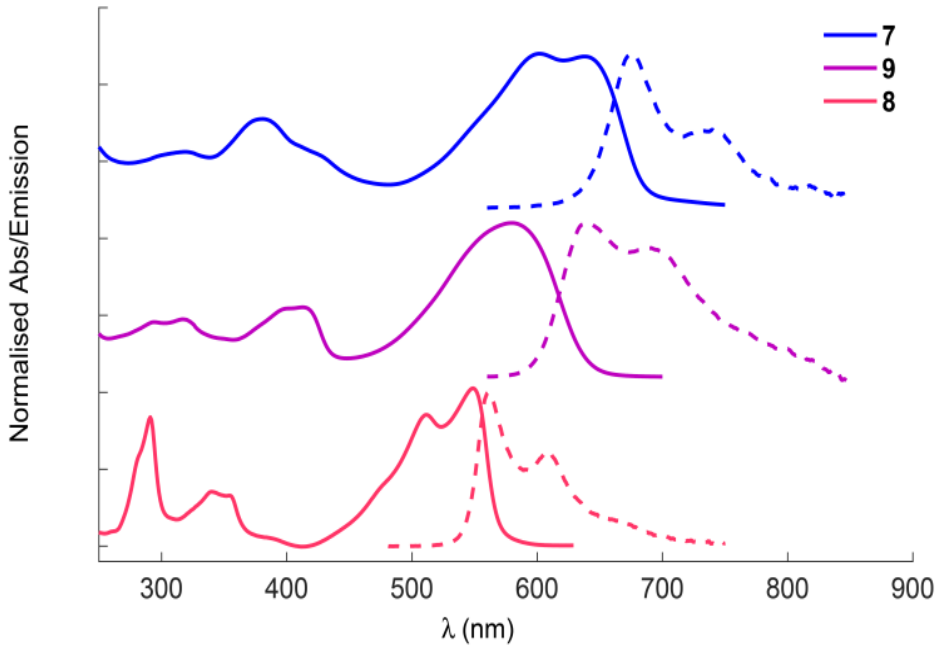

Figure 2. Absorption (solid lines) and emission (dashed lines) spectra of compounds 7-9 as solutions in CH_2Cl_2.

Redox Properties. Cyclic voltammetry studies for **7**, **8** and **9** show two oxidation processes and either one (**8**) or two (**7** and **9**) reduction processes for each compound in the potential range between *ca*. +1.00 and -2.10 V versus Fc^{+}/Fc (Table 2). The first oxidation and reduction processes appear as redox couples in a range of scan rates between 0.02 and 0.30 Vs^{-1}. For **8** and **9** these reductions are essentially reversible, however the oxidations show variation in ΔE (= $E_p^a - E_p^c$) with scan rate greater than that observed for ferrocene under identical conditions. Hence, these couples appear electrochemically quasi-reversible. The CVs show **9** to have a significantly smaller energy-gap than that of **8** due to lower potentials for both reduction and oxidation processes. DPP **7** follows the same trend with a further decrease in the band-gap.

Table 2. Half-wave potentials relative to Fc^{+}/Fc for the first oxidation and reduction of compounds **7-9**.[a]

	$E_{1/2}^{red}$ (V)	$E_{1/2}^{ox}$ (V)	E_{onset}^{red} (V)	E_{onset}^{ox} (V)
8	−1.60 (0.07)	+0.51 (0.07)	−1.49	+0.43
9	−1.49 (0.08)	+0.42 (0.08)	−1.36	+0.31
7	−1.44 (0.10)	+0.34 (0.12)	−1.32	+0.21

[a] Potentials reported as E1/2 (= (Epa + Epc)/2) in V vs. Fc+/Fc at 0.1 Vs-1 scan rate and quoted to the nearest 0.01 V. Values in parentheses are ΔE (= Epa – Epc) for the couple at 0.01 Vs-1. ΔE(Fc+/Fc) was 0.07 V under these conditions.

Electronic Structure Calculations. Singlet gas-phase geometry optimisations and subsequent TD-DFT calculations with the B3LYP hybrid functional and the 6-311G(d,p) basis set[42-44] gave calculated orbital eigenvalues and positions of the absorption maxima relatively close to those obtained from experiment (see Supporting Information). Generally, the higher energy absorptions could not be assigned to single orbital transitions due to several contributions to the configuration-interaction (CI) expansions of the excited states. However the peak at 381 nm in the absorption spectra

of **7** could be well approximated as arising from the HOMO−1⟶LUMO+1 transition as this excitation possessed a CI expansion coefficient of 0.65, with the next largest coefficient being 0.11. In this case, both contributing orbitals are primarily localised on thiophene units.

X-Ray Crystallography. Growth of single crystals of DPP **9** allowed a study of the position and conformation of the chiral group in the solid state by X-ray diffractometry. Despite significant effort. Compound **9** formed polar crystals pertaining to the triclinic space group *P*1 (Figure 3). The terminal thiophene ring exists in two distinct geometries with respect to the aromatic core and the structure was refined accordingly. Two dimensional layers are formed, with successive layers separated by a region populated by the hexyl chains and the myrtenal-derived aliphatic framework. Each molecule has both π-π stacking (3.4-3.6 Å) and lateral contacts with approximately coplanar neighbours (2.4-2.9 Å). Slipped packing is observed, with adjacent lactam units interacting with thiophene rings on opposing faces of the DPP core.

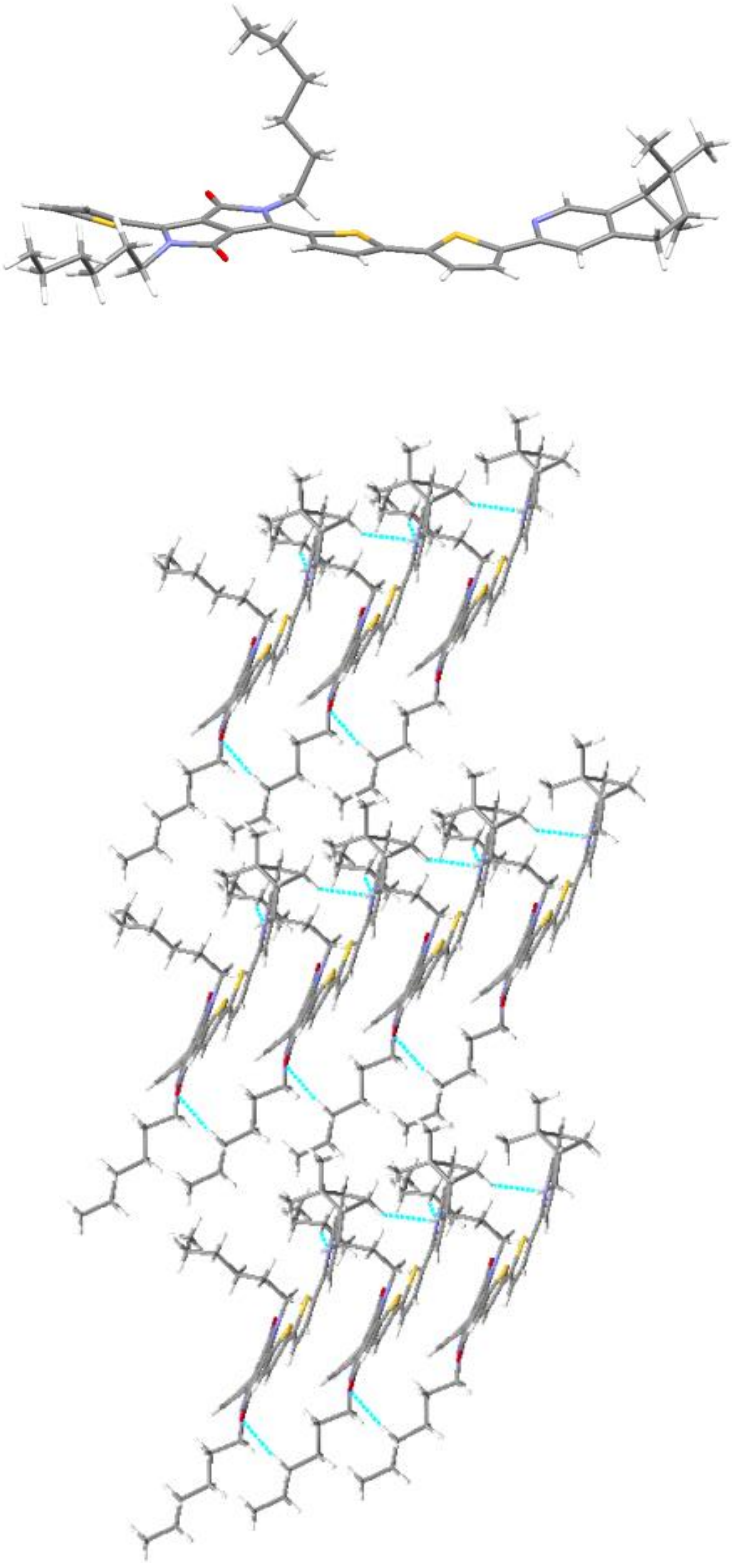

Figure 3. Crystal structure of compound 9. Top = a single molecule. Below = a view of the polar stack. A single thiophene geometry is shown.

Self-Assembly. Self-assembly of the compounds was probed using circular dichroism (CD) spectroscopy, in which molecular solutions of **7** and **9** in THF have weak negative Cotton effects at 240 nm and 238 nm, respectively, with no other significant features (see supporting information). Several solvents (MeOH, MeCN, methylcyclohexane) and combinations thereof were examined to test their ability to induce aggregation, and at concentrations suitable for CD measurements (~10^{-5} M). Aggregation was only detected for **7** when a solution of the compound in THF was injected into a mixture of THF and methanol so the final ratio of THF:MeOH was 7:3 ($c = 2 \times 10^{-5}$ M).

Temperature-dependent CD of **7** in solution (Figure 4) gives the largest peak at 712 nm, corresponding to a small shoulder in the absorption signal which evolves linearly with CD intensity over the range 30-60 °C ($R^2 = 0.9944$). A negative signal extending into the near infra-red region is observed, reaching maximum intensity at approximately 880 nm. This is accompanied by a comparatively small increase in absorbance at these wavelengths. These features indicate coupling between delocalised π-orbitals and the formation of ordered chiral aggregates. The positive Cotton effect present at 712 nm overlaps with a broad peak at 616 nm, which is located approximately halfway between the two absorption maxima corresponding to the HOMO-LUMO transition, which occur at 636 and 600 nm in THF/ MeOH at 20 °C. Notably, this peak does not exhibit excitonic coupling, indicating a lack of association between the DPP chromophores in the aggregated state. This feature is reminiscent of the crystal structure of DPP **9**. In addition, there is a bisignate band centred at 372 nm. The assignment of the corresponding absorption peak using TD-DFT indicated coupling between stacked thiophene units, rotated relative to one another. The CD signal is lost upon heating of the solution to 60 °C and is not recovered when the solution was cooled to 20 °C, indicating that the aggregates are formed under kinetic rather than thermodynamic conditions.[45] No aggregation in solution was observed for DPP **9** in any of the solvent systems investigated for **7**. At concentrations suitable for CD, 9 was soluble in DCM, chloroform, toluene and THF. To induce aggregation methanol, acetonitrile and

methylcyclohexane were tested but none was observed. We also tested latter three solvents almost neat by diluting a tiny amount of dissolved compound in THF with the precipitating solvent.

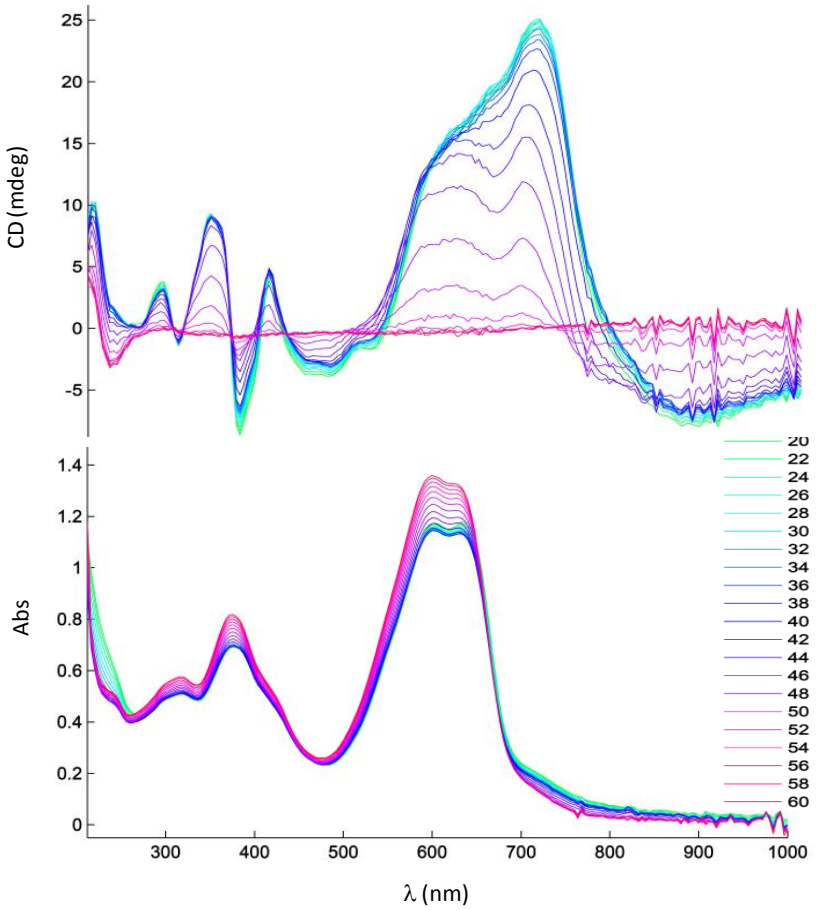

Figure 4. Circular dichroism and associated absorbance spectra of DPP 7 in THF/ MeOH 7:3 (2 × 10−5 M) and at temperatures from 20 °C to 60 °C.

CD measurements were also conducted on thin-films of **7** and **9** prepared by casting dichloromethane solutions of the compounds onto quartz substrates (Figure 5). Interestingly, **9** displayed more intense differential absorption than **7**. The CD exhibited by films of **9** is consistent with chiral order. The thin-film spectrum of DPP **7** also displayed features indicating chiral organisation, although with markedly lower intensity. Differential absorption extends into the near-IR, reaching a maximum intensity at 757 nm. Interestingly, the long wavelength CD signal is opposite to that observed in solution.

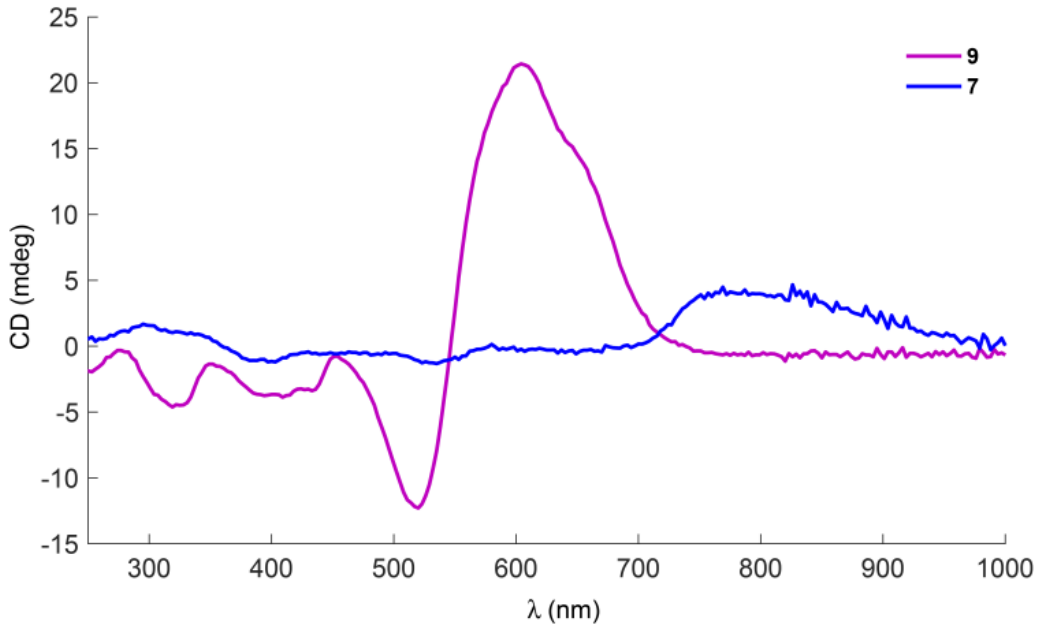

Figure 5. Circular dichroism spectra of DPPs 7 and 9 as thin-films.

Photovoltaic Performance. The performance of DPP **7** and DPP **9** as donors in OPV devices was investigated, employing $PC_{61}BM$ as the acceptor. The device configuration was ITO/ PEDOT:PSS/ photoactive layer/ Al (ITO = indium tin oxide, PEDOT:PSS is poly(3,4-ethylenedioxythiophene) poly-styrene sulfonate). Bulk heterojunction cells were prepared by spin-coating solutions containing both the donor and acceptor. Parameters for all fabrication conditions which produced working solar cells can be found in the Supporting Information. Initially, a solution of DPP **7** and $PC_{61}BM$ 1:1 (wt.) 1% (wt.) in chlorobenzene was deposited. However the resultant films displayed very little visible colour, which was attributed to a large disparity between the solubility of **7** and $PC_{61}BM$ in chlorobenzene (the latter is significantly more soluble in chlorobenzene) leading to a high degree of phase separation and particles of dye. Blend layers prepared using a 1:1 (wt.) (1 wt.%) mixture of **7** and $PC_{61}BM$ in chloroform resulted in more uniform and absorbent films. The possible reasons for this effect are discussed below (see section on film morphology).

Devices were prepared with a variety of active layer spin-casting speeds (Supporting information). It was found that power conversion efficiency (PCE) and short-circuit current density (J_{SC}) increased with spin-rate, scaling

inversely with layer thickness/solvent evaporation rate. This trend suggests that DPP **7** exhibits poor bulk conductivity, which could be due to a poor charge mobility, high recombination, high density of trap states or any combination of these factors, as the gain in extracted photocurrent from a smaller distance travelled through the medium outweighs the loss from a thinner layer absorbing less light. In contrast, the open circuit voltage (V_{OC}) scaled inversely with film thickness (determined by spin-rate). The most efficient device was prepared by spin-coating the photoactive layer at 2000 rpm, for which PCE = 0.05%, V_{oc} = 0.10 V, fill factor (FF) = 26% and J_{SC} = −2.05 μA/cm^{2,} (the *J-V* curve is shown in Figure 6). Thermal annealing at 125 °C for 10 minutes had no effect on device performance. These values are substantially lower than P3HT/$PC_{61}BM$ devices prepared in our laboratory under identical conditions as a reference (for which PCE = 1.03%).

In contrast to DPP **7**, DPP **9** exhibited higher solubility in chlorobenzene and films that were prepared by spin-casting from blends prepared from it exhibited strong coloration, so all blends of DPP **9**:$PC_{61}BM$ employed in subsequent device measurements were prepared from this solvent. For this compound, we explored the effect of decreasing the donor/acceptor ratio in addition to spin rate (for film thicknesses see Supporting Information). For blend ratios of 1:1, 1:2 and 1:3 (by weight), PCE and J_{sc} increased with increasing spin-rate, correlating with decreasing layer thickness. In contrast, for a donor:acceptor ratio of 1:5, PCE and J_{sc} decreased with increasing spin rate.

The best device performance in terms of PCE was achieved by using a 1:3 ratio of **9**/$PC_{61}BM$ and spin coating at 2500 rpm. Cells prepared under these conditions exhibited V_{oc} = 0.20V, J_{SC} = −0.65 mA/cm^2, FF = 33 % and PCE of 0.04 %. The biggest factor in the poor performance appears to be the very low J_{sc}. The most obvious explanation for this effect would be that, as with DPP **7**, the blend exhibits low bulk conductivity. The *J-V* curve for this cell (shown in Figure 6) shows imperfect diode behaviour, with negative current density substantially increasing at voltages lower than -1.5 V.

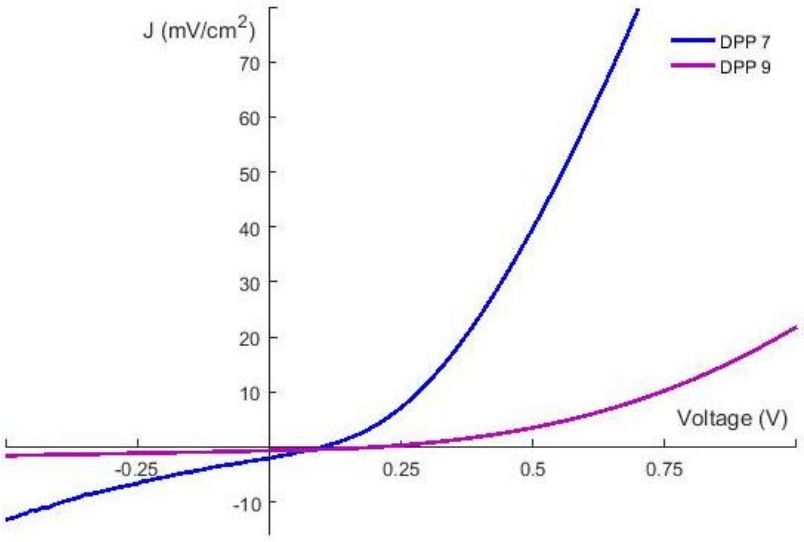

Figure 6. J-V curve plotting current density (J) against Voltage (V) of best performing devices fabricated using DPP 7:PC61BM and DPP 9:PC61BM.

Both materials were able to produce devices with V_{oc} = ca. 0.3 V in certain conditions (see supporting information). While this is less than the literature values for known materials (ca. 0.6 V is typical for P3HT:PC61BM) it is high enough to strongly imply that there is significant charge carrier generation in the blend under illumination. However the J_{sc} of almost all devices was between 0 and -1 mA/cm^2 (ca. 10 mA/cm^2 is seen with well-performing P3HT:PC_{61}BM devices) and the FF was usually less than 30 (above 60 is often seen for P3HT:PC_{61}BM) which strongly implies that very little of the generated charge was extracted, leading to a low PCE.

Film Morphology. The active layer morphology of devices containing **7** and PC_{61}BM was probed using atomic force microscopy (AFM). Qualitatively it appears that clumps of material form on the surface, in lower quantity but greater size in the sample spun-cast from chloroform compared to the sample spun-cast from chlorobenzene (see Figure 7).

Furthermore it was found that samples cast from $CHCl_3$ exhibited smoother surface topography (RMS roughness = 0.22 nm, mean value calculated from several images) compared with those prepared from chlorobenzene (RMS roughness = 0.47 nm). This observation implies that phase separation of the

active components is less pronounced in the film prepared from chloroform as a lower surface roughness is linked to smaller domain sizes.[46] Both the smaller disparity in the relative solubility of the two components in chloroform and the lower evaporation time from this more volatile solvent would contribute to this effect.

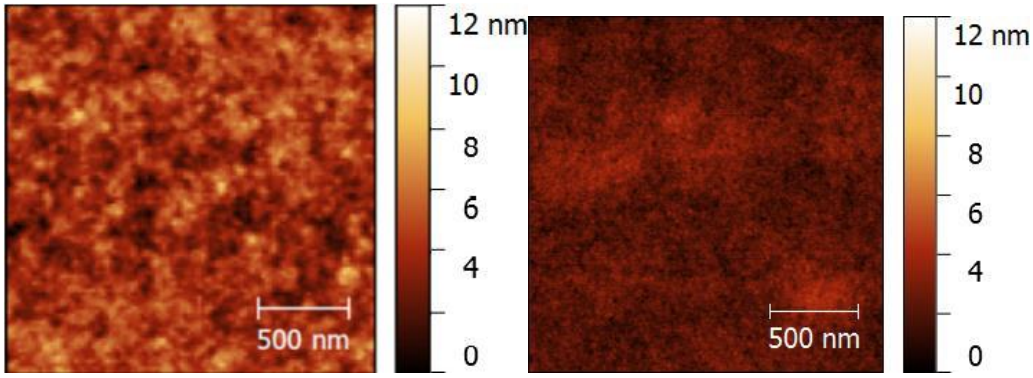

Figure 7. AFM images of films spin-cast from 1:1 blends of 7 and PC61BM in chlorobenzene (left) and chloroform (right).

Smaller domain sizes of DPP **7** would also be expected to lead to more intense coloration of the blend thin film, as was observed as samples spun-cast from chloroform had much more intense colour than those cast from chlorobenzene. The effect of thermal annealing on the blends containing DPP **9** and $PC_{61}BM$ was investigated, however it was found that it led to the formation of very large crystalline domains clearly visible by optical microscopy (see Figure 8). For this reason, thermal annealing was not used in the preparation of devices, as bulk heterojunctions require much smaller domain sizes.

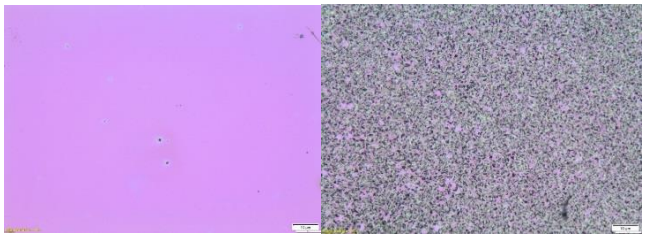

Figure 8. Optical microscope images of films spin-cast from 1:1 blends of DPP 9 and PC61BM in chlorobenzene with no thermal annealing (left) and annealed at 125°C under a nitrogen atmosphere for 10 min (right).

The mean RMS roughness calculated from several images of an annealed sample of a film prepared from a 1:1 ratio blend if DPP **9** and $PC_{61}BM$ was 0.45 nm compared to 0.27 nm for an equivalent non-annealed sample. AFM images of both an annealed and non-annealed sample show a proliferation of nanocrystalline structures in the film, unlike those prepared using DDP **7** and $PC_{61}BM$, showing that DPP **9** is more inclined towards ordered crystallite formation under the spin-casting conditions of the compounds described here (see Figure 9).

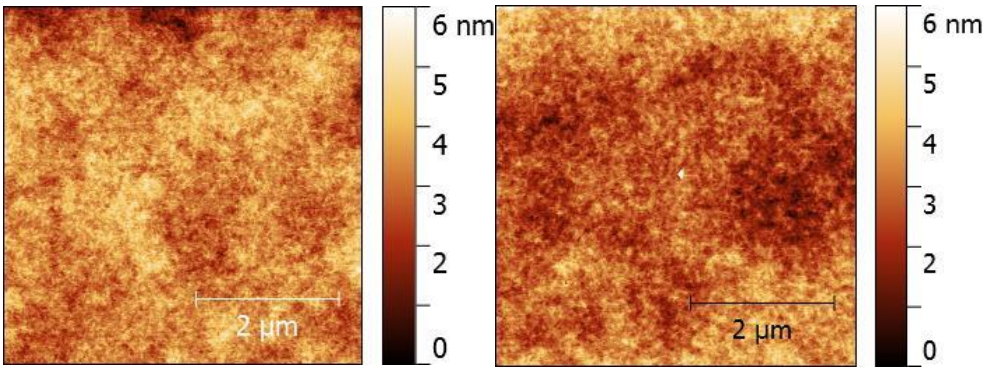

Figure 9. AFM images of films spin-cast from 1:1 blends of 9 and PC61BM in chlorobenzene with no thermal annealing (top) and annealed at 125°C under a nitrogen atmosphere for 10 min (bottom).

Conclusions

The novel class of chiral DPP-based molecular materials reported herein show how the chiral at-end strategy is a way to influence the organisation of optically active aggregates of chromophores. In this case, chiral substitution at both "ends" is necessary to create significant optical activity in solution for the C_2 symmetric compound, although as a thin film the asymmetric compound with a single stereogenic group shows greatest optical activity. The results demonstrate that CD is an extremely sensitive probe for the organisation of these compounds, as very modest changes in the absorption spectra are noted, making the chiral structures useful for the understanding of related self-assembled structures in general. The (1*R*)-(−)-myrtenal might at first sight seem so large that it would encumber π-π interactions, but this

was proved not to be the case in the X-ray crystal structure of the asymmetric molecule.

OPV devices preparedemploying these DPP materials as donors and $PC_{61}BM$ as an acceptor gave very low PCE and J_{sc}, around an order of magnitude lower than devices made with P3HT:$PC_{61}BM$ under similar conditions. The main reason for the poor performance is likely to be low charge carrier mobility of the materials. Mobility in chiral materials is known to be extremely sensitive to supramolecualr organisation.[47] Morphological analysis revealed that the asymmetric compound is the more inclined to form ordered crystalline domains when spun-cast as a blend with $PC_{61}BM$, which could be of interest for larger molecules based on similar materials with greater charge transport.[48-50]

Experimental Section

General Methods: Commercially available reagents and solvents were used as received. Unless otherwise noted, all reactions were performed under an atmosphere of argon. THF used in reactions was dried and purified by passage through activated alumina columns using a solvent purification system. All other reagents were used as received unless otherwise noted. Reactions were monitored by thin-layer chromatography (TLC) carried out on E. Merck silica gel plates using UV light and developed with potassium permanganate where appropriate. Flash column chromatography was carried out using either silica (Sigma-Aldrich, pore size 60 Å, particle size 40-63 µm) or activated alumina gel (Sigma-Aldrich, neutral, pore size 58Å, Brockman I). Size exclusion chrmoatography was performed using Bio-Beads™ S-X1 beads (200-400 mesh).

NMR spectra were acquired on a Jeol EX270, Bruker DPX300, Bruker AV400, Bruker DPX400, or a Bruker AV(III)500 spectrometer. ^{1}H and ^{13}C NMR spectra were referenced to the residual protonated solvent (^{1}H) or the solvent itself (^{13}C). NMR spectra were recorded at room temperature in $CDCl_3$

solutions. Chemical shifts are reported in parts per million (ppm). Coupling constants, *J*, quoted to the nearest 0.1 Hz. Multiplicities are reported as "s" (singlet), "br s" (broad singlet), "d" (doublet), "dd" (doublet of doublets), "ddd" (doublet of doublets of doublets), "t" (triplet) and "m" (multiplet). Infra-red spectra were recorded on a Bruker Tensor 27 instrument equipped with a Pike GladiATR attachment with a diamond crystal. Optical rotations were performed on a Bellingham and Stanley ADP410 polarimeter, using the sodium-D line (589 nm) and concentration measured in grams per 100 mL. Melting points were determined on a Gallenkamp melting point apparatus and are uncorrected. High resolution mass spectra were recorded using electrospray ionization (ESI) techniques at the School of Chemistry, University of Nottingham. Elemental analyses (CHN) were performed by the University of Nottingham, School of Chemistry Microanalytical Service on an Exeter Analytical CE-440 instrument.

Absorption and fluorescence spectra were obtained using a PerkinElmer Lambda 25 UV/Vis spectrometer and a FluoroMax-3® spectrometer respectively. Cyclic voltammetric studies were carried out using an Autolab PGSTAT20 potentiostat. Standard cyclic voltammetry was carried out under an atmosphere of argon using a three-electrode arrangement in a single compartment cell. A glassy carbon working electrode, a Pt wire secondary electrode and a saturated calomel reference electrode, chemically isolated from the test solution via a bridge tube containing electrolyte solution and fitted with a porous Vycor frit, were used in the cell. Redox potentials are quoted versus the ferrocenium-ferrocene couple used as an internal reference.[46] Compensation for internal resistance was not applied.

Circular dichroism spectra were recorded on an Applied Photophysics Chirascan plus spectrometer using high-precision, spectrally matched quartz cuvettes with a path length of 10 mm. Thin film measurements were conducted on quartz substrates and the CD spectra averaged over 4

orientations in order to compensate for any linear dichroic effects in the plane of the film.

Current-voltage characteristics of OPV devices were recorded with a Keithley 2401 sourcemeter.

Synthetic Procedures

(6*R*,8*R*)-7,7-dimethyl-3-(thiophen-2-yl)-5,6,7,8-tetrahydro-6,8-methanoisoquinoline (3)

To a stirred solution of pyridinium salt **2** (2.00g, 6.04 mmol) in formamide (7 mL) at room temperature was added ammonium acetate (930 mg, 12.1 mmol) in one portion. The resultant solution was heated to 50 °C and stirred for 30 min. (1*R*)-(−)-Myrtenal (0.97 mL, 6.34 mmol) was added dropwise over 5 minutes and the solution heated to 60 °C for 12 h. The reaction mixture was cooled to room temperature, quenched by the addition of water (50 mL) and then extracted with hexanes (3 × 20 mL). The combined organic extracts were dried over $MgSO_4$ and concentrated *in vacuo*. Purification of the product by column chromatography (hexanes/ EtOAc 3:1) afforded the *title compound* **3** as a white solid (1.39 g, 5.44 mmol, 90%). m.p. 116.5-117.5 °C; $[\alpha]_D^{25}$ = −63.7 (*c* = 1.1 in $CHCl_3$); ^{1}H NMR (400 MHz, $CDCl_3$): δ 8.12 (1H, s, Ar-H), 7.56 (1H, dd, *J* = 3.7, 1.2 Hz, Ar-H), 7.48 (1H, s, Ar-CH), 7.36 (1H, dd, *J* = 5.1, 1.1 Hz, Ar-CH), 7.11 (1H, dd, *J* = 5.1, 3.7 Hz, Ar-CH), 3.02 (2H, dd, CH_2), 2.85 (1H, dd, *J* = 5.5, 5.5 Hz, CH), 2.75-2.68 (1H, m, CH_2), 2.35-2.29 (1H, m, CH), 1.43 (3H, s, CH_3), 1.24 (1H, d, *J* = 9.6 Hz, CH_2); ^{13}C NMR (100 MHz, $CDCl_3$): δ 150.5 (Ar-C), 145.7 (Ar-C), 145.2 (Ar-CH), 144.9 (Ar-C), 141.3 (Ar-CH), 127.9 (Ar-CH), 126.8 (Ar-CH), 123.9 (Ar-CH), 118.5 (Ar-CH), 44.4 (CH), 40.0 (CH), 39.4 (C), 32.9 (CH_2), 31.9 (CH_2), 26.0 (CH_3), 21.4 (CH_3); IR (film) ν_{max} 2998, 2945, 2908, 1600, 1551, 1537, 1476, 1388, 1227, 1217, 1055, 855, 814, 757, 707 cm^{-1}; HRMS (ESI+) for $C_{16}H_{17}NNaS$ $[M+Na]^+$ requires 256.1154 found 256.1155.

(6*R*,8*R*)-3-(5-bromothiophen-2-yl)-7,7-dimethyl-5,6,7,8-tetrahydro-6,8-methanoisoquinoline (4)

To a stirred solution of thiophene **3** (500 mg, 1.96 mmol) in $CHCl_3$ (20 mL) was added *N*-bromosuccinimide (384 mg, 2.16 mmol). The resultant solution was heated to 50 °C for 24 h. The reaction mixture was allowed to cool to room temperature, quenched with water (20 mL) and extracted with CH_2Cl_2 (3 × 20 mL). The combined organic extracts were dried over $MgSO_4$ and concentrated *in vacuo*. Purification by column chromatography (CH_2Cl_2) afforded **4** as a white solid (645 mg, 1.93 mmol, 99%). m.p. 110.5-113.5 °C; $[\alpha]_D^{25}$ = −46.8 (*c* = 0.26 in $CHCl_3$); ^{1}H NMR (400 MHz, $CDCl_3$): δ 8.08 (1H, s, Ar-H), 7.39 (1H, s, Ar-H), 7.28 (1H, d, *J* = 3.9 Hz, Ar-H), 7.05 (1H, d, *J* = 3.9 Hz, Ar-H), 3.01 (2H, d, *J* = 3.9 Hz), 2.84 (1H, dd, *J* = 5.5, 5.5 Hz, CH), 2.75-2.70 (1H, m, CH_2), 2.35-2.30 (1H, m, CH_2), 1.43 (3H, s, CH_3), 1.23 (1H, d, 9.6 Hz, CH_2), 0.68 (3H, s, CH_3); ^{13}C NMR (100 MHz, $CDCl_3$): δ 149.9 (Ar-C), 146.7 (Ar-C), 145.9 (Ar-C), 145.5 (Ar-CH), 141.9 (Ar-C), 130.9 (Ar-CH), 123.8 (Ar-CH), 117.9 (Ar-CH), 114.2 (Ar-C), 77.4 (Ar-C), 44.6 (CH), 40.1 (CH), 39.5 (C), 33.0 (CH_2), 31.9 (CH_2), 26.1 (CH_3), 21.5 (CH_3); IR (film) ν_{max} 2935, 1599, 1478, 1436, 1388, 1004, 963, 865, 804, 756 cm^{-1}; HRMS (ESI+) for $BrC_{16}H_{16}NNaS$ $[M+Na]^+$ requires 334.0260 found 334.0260.

(6*R*,8*R*)-7,7-dimethyl-3-(5-(4,4,5,5-tetramethyl-1,3,2-dioxaborolan-2-yl)thiophen-2-yl)-5,6,7,8-tetrahydro-6,8-methanoisoquinoline (5)

To a stirred solution of $[Ir(COD)OMe]_2$ (1.3 mg, 2 µmol) and 4,4′-di-*tert*-butyl-2,2′-dipyridyl (1.0 mg, 4 µmol) in heptane (2 mL) under argon was added pinacolborane (0.17 mL, 1.17 mmol) resulting in the formation of a deep red solution. Thiophene 3 (200 mg, 780 µmol) was added in one portion and the reaction mixture heated at 80 °C for 24 h. The reaction mixture was allowed to cool to room temperature, filtered through Celite® and then concentrated *in vacuo*. The crude product **5** thus obtained was used directly without further purification.

3,6-bis(5'-((6*R*,8*R*)-7,7-dimethyl-5,6,7,8-tetrahydro-6,8-methanoisoquinolin-3-yl)-[2,2'-bithiophen]-5-yl)-2,5-dihexyl-1,4-diketopyrrolo[3,4-*c*]pyrrole (7)

Under an atmosphere of argon, a stirred mixture of bromide **6** (100 mg, 160 µmol), boronate **5** (200 mg, prepared above), $Pd(PPh_3)_4$ (7.0 mg, 6.4 µmol) and potassium carbonate (0.8 mL, 2 M aq.) in THF (2 mL) was heated at 80 °C for 4 h. A further portion of $Pd(PPh_3)_4$ (7.0 mg, 6.4 µmol) was added and heating continued for a further 16 h. The reaction mixture was allowed to cool to room temperature, diluted with brine (10 mL) and extracted with CH_2Cl_2 (3 × 10 mL). The combined organic extracts were dried over $MgSO_4$ and concentrated *in vacuo*. Sequential purification by column chromatography (CH_2Cl_2 containing 0.1%⟶5% v/v THF) and size-exclusion chromatography ($CHCl_3$) afforded the *title compound* **7** as a blue powder (59 mg, 60.8 µmol, 38%); m.p. > 250 °C; ^{1}H NMR (400 MHz, $CDCl_3$): δ 8.96 (2H, d, J = 4.2 Hz, Ar-H 2), 8.11 (2H, s, Ar-H × 2), 7.45-7.43 (2H, m, Ar-H × 4), 7.36 (2H, d, J = 4.2 Hz, Ar-H × 2), 7.30 (2H, d, J = 3.9 Hz, Ar-H × 2), 4.09 (4H, t, J = 8.0 Hz, NCH_2 × 2), 3.00 (4H, s, CH_2 × 2), 2.84 (2H, dd, J = 5.4, 5.4 Hz CH × 2), 2.74-2.69 (2H, m, H of CH_2 × 2), 2.33-2.30 (2H, m, CH × 2), 1.80-1.74 (4H, m, CH_2 × 2), 1.47-1.34 (18H, m, CH_3 × 2, CH_2 × 6), 1.23 (2H, d, J = 8.0 Hz, H of CH_2 × 2), 0.67 (6H, s, CH_3 × 2); ^{13}C NMR (100 MHz, $CDCl_3$): δ 161.4 (C=O), 150.1 (Ar-C), 146.3 (Ar-C), 145.9 (Ar-CH), 145.5 (Ar-C), 143.2 (Ar-C), 142.0 (Ar-C), 139.1 (Ar-C), 137.1 (Ar-C), 136.9 (Ar-CH), 128.3 (Ar-C), 126.1 (Ar-CH), 125.2 (Ar-CH), 124.5 (Ar-CH), 118.3 (Ar-CH), 108.4 (Ar-C), 44.7 (CH), 42.5 (CH_2), 40.2 (CH), 39.5 (C), 33.0 (CH_2), 32.0 (CH_2), 31.6 (CH_2), 30.2 (CH_2), 26.8 (CH_2), 26.1 (CH_3), 22.7 (CH_2), 21.6 (CH_3), 14.2 (CH_3); IR (film) ν_{max} 2923, 1467, 1597, 1549, 1427, 1212, 1082, 1023, 947, 802, 732 cm^{-1}; HRMS (ESI+) Anal. Calcd for $C_{58}H_{62}N_4O_2S_4$: C, 71.42; H, 6.41; N, 5.74. Found: C, 71.14; H, 6.61; N, 5.56.

3-(5'-((6*R*,8*R*)-7,7-dimethyl-5,6,7,8-tetrahydro-6,8-methanoisoquinolin-3-yl)-[2,2'-bithiophen]-5-yl)-2,5-dihexyl-6-(thiophen-2-yl)-1,4-diketopyrrolo[3,4-*c*]pyrrole (9)

Under an argon atmosphere, a mixture of thiophene-DPP **8** (140 mg, 300 µmol), bromothiophene 4 (100 mg, 300 µmol), $Pd(OAc)_2$ (3.4 mg, 15 µmol), pivalic acid (9.0 mg, 90 µmol) and potassium carbonate (62 mg, 450 µmol) in dimethylacetamide (3 mL) was heated at 100 °C for 24 h with stirring. The

reaction mixture was allowed to cool to room temperature, diluted with brine (10 mL) and then extracted with CH_2Cl_2 (3 × 10 mL). The combined organic extracts were dried over $MgSO_4$ and then concentrated *in vacuo*. Purification by column chromatography (CH_2Cl_2 containing 0.1% v/v THF, 0.25% NEt_3) afforded the *title compound* **9** as a purple solid (39 mg, 54 µmol, 18%); m.p. 159-163 °C; ^{1}H NMR (400 MHz, $CDCl_3$): δ9.00 (1H, d, J = 4.2 Hz, Ar-H), 8.94 (1H, dd, J = 3.9, 1.2 Hz, Ar-H), 8.14 (1H, s, Ar-H), 7.65 (1H, dd, J = 5.0, 1.1 Hz, Ar-H), 7.50-7.43 (2H, m, Ar-H × 2), 7.41 (1H, d, J = 4.0 Hz, Ar-H), 7.35 (1H, d, J = 3.8 Hz, Ar-H), 7.30 (1H, dd, J = 5.0, 4.1 Hz, Ar-H), 4.13-4.08 (4H, m, NCH_2 × 2), 3.04 (2H, d, J = 2.9 Hz, CH_2), 2.87 (1H, t, J = 5.0 Hz, CH), 2.77-2.72 (1H, m, CH of CH_2), 2.36-2.33 (1H, m, CH), 1.82-1.74 (4H, m, CH_2 × 2), 1.50-1.25 (16H, m, CH_3, CH_2 × 6, CH of CH_2), 0.94-0.89 (6H, m, CH_3 × 2), 0.70 (3H, s, CH_3); ^{13}C NMR (100 MHz, $CDCl_3$): δ 161.6 (C=O), 161.3 (C=O), 150.1 (Ar-C), 146.5 (Ar-C), 146.0 (Ar-CH), 145.5 (Ar-C), 143.4 (Ar-C), 142.1 (Ar-C), 139.8 (Ar-C), 139.5 (Ar-C), 137.0 (Ar-CH), 137.0 (Ar-C), 135.3 (Ar-CH), 130.6 (Ar-CH), 130.0 (Ar-C), 128.8 (Ar-CH), 128.2 (Ar-C), 126.1 (Ar-CH), 125.2 (Ar-CH), 124.4 (Ar-CH), 118.3 (Ar-CH), 108.1 (Ar-C), 108.1 (Ar-C), 44.7 (CH), 42.4 (CH_2), 40.2 (CH), 39.5 (C), 33.0 (CH_2), 32.0 (CH_2), 31.6 (CH_2), 31.6 (CH_2), 30.2 (CH_2), 30.1 (CH_2), 26.7 (CH_2), 26.7 (CH_2), 26.1 (CH_3), 22.7 (CH_2 × 3), 21.6 (CH_3), 14.2 (CH_3), 14.2 (CH_2); IR (film) ν_{max} 2924, 2856, 1793, 1599, 1553, 1424, 1407, 1230, 1104, 1083, 1030, 732 cm^{-1}; HRMS (ESI+) Anal. Calcd for $C_{42}H_{47}N_3O_2S_3$: C, 69.87; H, 6.56; N, 5.82. Found: C, 69.93; H, 6.66; N, 5.75.

General OPV device fabrication procedure

Active blend solutions were stirred overnight at 50°C. The ITO on glass substrates (Diamond coatings) were cleaned by sonication sequentially in Hellmanex (III) solution (1% aq.) for 5 minutes, acetone for 5 minutes and two portions of 2-propanol for 10 minutes each, rinsing with deionised water between each step. The substrates were then stored underwater until drying by spinning at 5000 rpm for 30 s, followed by treatment with UV/ozone for 20 minutes.

PEDOT:PSS was filtered using a PVDF syringe filter (0.22 µm) and spun-cast dynamically at 5000 rpm for 30 seconds and the samples heated at 150°C on a hotplate until needed for active layer deposition. The active layer solution was filtered with a PTFE syringe filter (0.22 µm) and dynamically spun-cast at 550 rpm for 30 seconds then 2000 rpm for 45 seconds. The samples were then transferred to a nitrogen glovebox and 100 nm of elemental Al deposited by thermal evaporation. *J-V* curves were recorded under AM 1.5 1 sun illumination in air.

Acknowledgements

We thank the EPSRC, GSK, and the School of Chemistry at the University of Nottingham for funding, and Prof. Jonathan McMaster for assistance with calculations.

References

[1] M. Liu, L. Zhang, T. Wang, *Chem. Rev.*, **2015**, *115*, 7304.

[2] F.R. Keene (Ed.) *Chirality in Supramolecular Assemblies: Causes and Consequences*, Wiley, 2017.

[3] I. D. Tevis, W. W. Tsai, L. C. Palmer, T. Aytun, S. I. Stupp, *ACS Nano*, **2012**, *6*, 2032.

[4] T. Ikai, R. Kojima, S. Katori, T. Yamamoto, T. Kuwabara, K. Maeda, K. Takahashi, S. Kanoh, *Polymer*, **2015**, *56*, 171.

[5] R. B. Zerdan, N. T. Shewmon, Y. Zhu, J. P. Mudrick, K. J. Chesney, J. G. Xue, R. K. Castellano, *Adv. Funct. Mater.*, **2014**, *24*, 5993.

[6] D. Ley, C. X. Guzman, K. H. Adolfsson, A. M. Scott, A. B. Braunschweig, *J. Am. Chem. Soc.*, **2014**, *136*, 7809.

[7] Y. Yang, B. Rice, X. Y. Shi, J. R. Brandt, R. C. da Costa, G. J. Hedley, D. M. Smilgies, J. M. Frost, I. D. W. Samuel, A. Otero-De-La-Roza, E.

R. Johnson, K. E. Jelfs, J. Nelson, A. J. Campbell, M. J. Fuchter, *ACS Nano,* **2017**, *11*, 8329.

[8] C. Sooambar, V. Troiani, H. Qiu, S. Fukuzumi, L. Flamigni, R. Rein, N. Solladié, *J. Porph. Phthal.*, **2018**, *22*, 291.

[9] P.M. Beaujuge, J.M.J. Frechet, *J. Am. Chem. Soc.*, **2011**, *133*, 20009.

[10] J. L. Bredas, J. E. Norton, J. Cornil, V. Coropceanu, *Acc. Chem. Res.*, **2009**, *42*, 1691.

[11] F. Bruni, M. Sassi, M. Campione, U. Giovanella, R. Ruffo, S. Luzzati, F. Meinardi, L. Beverina, S. Brovelli, *Adv. Funct. Mater.*, **2014**, *24*, 7410.

[12] J.R. Tumbleston, B.A. Collins, L. Yang, A.C. Stuart, E. Gann, W. Ma, W. You, H. Ade, *Nature Photonics*, **2014**, *8*, 385.

[13] K. A. Mazzio, C. K. Luscombe, *Chem. Soc. Rev.*, **2015**, *44*, 78.

[14] Y. Xie, W. Wu, H. Zhu, J. Liu, W. Zhang, H. Tiana, W.-H. Zhu, *Chem. Sci.*, **2016**, *7*, 544-549.

[15] R. Singh, J. Lee, M. Kim, P.E. Keivanidis, K. Cho, J. Mater. Chem. A, **2017**, *5*, 210.

[16] S. Li, L. Ye, W. Zhao, H. Yan, B. Yang, D. Liu, W. Li, H. Ade, J. Hou, *J. Am. Chem. Soc.*, **2018**, *140*, 7159

[17] D.B. Amabilino, D.K. Smith, J.W. Steed, *Chem. Soc. Rev.*, **2017**, *46*, 2404

[18] C. Poelking, D. Andrienko, *J. Am. Chem. Soc.*, **2015**, *137*, 6320.

[19] C. Liu, S. Dong, P. Cai, P. Liu, S. Liu, J. Chen, F. Liu, L. Ying, T. P. Russell, F. Huang and Y. Cao, *ACS Appl. Mater. Interfaces*, **2015**, *7*, 9038.

[20] E. D. Glowacki, H. Coskun, M. A. Blood-Forsythe, U. Monkowius, L. Leonat, M. Grzybowski, D. Gryko, M. S. White, A. Aspuru-Guzik, N. S. Sariciftci, *Org. Electron.*, **2014**, *15*, 3521.

[21] N. T. Shewmon, D. L. Watkins, J. F. Galindo, R. B. Zerdan, J. Chen, J. Keum, A. E. Roitberg, J. Xue, R. K. Castellano, *Adv. Funct. Mater.*, **2015**, *25*, 5166.

[22] H. Burckstummer, E. V. Tulyakova, M. Deppisch, M. R. Lenze, N. M. Kronenberg, M. Gsanger, M. Stolte, K. Meerholz, F. Wurthner, *Angew. Chem., Int. Ed.*, **2011**, *50*, 11628.

[23] A. M. Haruk, J. M. Mativetsky, *Int. J. Mol. Sci.*, **2015**, *16*, 13381.

[24] K.-E. Hung, C.-E. Tsai, S.-L. Chang, Y.-Y. Lai, U-S. Jeng, F.-Y. Cao, C.-S. Hsu, C.-J. Su, Y.-J. Cheng, *ACS Appl. Mater. Interfaces*, **2017**, *9*, 43861.

[25] F.-C. Hsu, J.-L. Chen, C. Kashi, P.-W. Tsao, C.-Y. Yeh, T.-Y. Lin, Y.-F. Chen, J. Phys. Chem. C, 2017, 121, 20084.

[26] Y. N. Li, P. Sonar, L. Murphy, W. Hong, *Energy Environ. Sci.*, **2013**, *6*, 1684.

[27] C. B. Nielsen, M. Turbiez, I. McCulloch, *Adv. Mater.*, **2013**, *25*, 1859.

[28] D. Chandran, K. S. Lee, *Macromol. Res.*, **2013**, *21*, 272.

[29] A. Tang, C. Zhan, J. Yao, E. Zhou, *Adv. Mater.* **2017**, *29*, 1600013.

[30] Z.M. Hao, A. Iqbal, *Chem. Soc. Rev.*, **1997**, *26*, 203.

[31] E. D. Głowacki, H. Coskun, M. A.Blood-Forsythe, U. Monkowius, L. Leonat, M. Grzybowski, D. Gryko, M. S. White, A. Aspuru-Guzik, N. S. Sariciftci, *Org. Electronics*, **2014**, *15*, 3521.

[32] C. Fu, P.J. Beldon, D.F. Perepichka, *Chem. Mater.*, **2017**, *29*, 2979.

[33] F. Pop, W. Lewis, D.B. Amabilino, *CrystEngComm*, **2016**, *18*, 8933.

[34] Y. Suna, J. Nishida, Y. Fujisaki, Y. Yamashita, *Org. Lett.*, **2012**, *14*, 3356.

[35] Q. Liu, A. Surendran, K. Feron, S. Manzhos, X. Jiao, C.R. McNeill, S. E. Bottle, J. Bell, W. L. Leong, P. Sonar, *New J. Chem.*, **2018**, *42*, 4017.

[36] D. Drahonovsky, U. Knof, L. Jungo, T. Belser, A. Neels, G. C. Labat, H. Stoeckli-Evans, A. von Zelewsky, *Dalton. Trans.*, **2006**, 1444.

[37] T. M. Kadayat, C. Park, K. Y. Jun, T. B. Magar, G. Bist, H. Y. Yoo, Y. Kwon, E. S. Lee, *Bioorg. Med. Chem.*, **2015**, *23*, 160.

[38] I. A. Mkhalid, J. H. Barnard, T. B. Marder, J. M. Murphy, J. F. Hartwig, *Chem. Rev.*, **2010**, *110*, 890.

[39] C. Kanimozhi, P. Balraju, G. D. Sharma, S. Patil, *J. Phys. Chem. B*, **2010**, *114*, 3095.

[40] L. G. Mercier, M. Leclerc, *Acc. Chem. Res.*, **2013**, *46*, 1597.

[41] Z. Chen, V. Stepanenko, V. Dehm, P. Prins, L. D. Siebbeles, J. Seibt, P. Marquetand, V. Engel, F. Wurthner, *Chem. Eur. J.*, **2007**, *13*, 436.

[42] A. D. Becke, *Phys. Rev. A*, **1988**, *38*, 3098.

[43] W. Yang, C. Lee, R. G. Parr, *Phys. Rev. B*, **1988**, *37*, 785.

[44] A. D. Becke, *J. Chem. Phys.*, **1993**, *98*, 5648.

[45] I. Danila, F. Pop, C. Escudero, L. N. Feldborg, J. Puigmarti-Luis, F. Riobe, N. Avarvari, D. B. Amabilino, *Chem. Commun.*, **2012**, *48*, 4552.

[46] L. Zhang, M. Pu, W. Zhou, X. Hu, Y. Zhang, Y. Xie, B. Liu, Y. Chen, *J. Phys. Chem. C*, **2015**, *119*, 23310.

[47] N. Avarvari, J.D. Wallis, *J. Mater. Chem.*, **2009**, *19*, 4061.

[48] D. Deng, Y. Zhang, J. Zhang, Z. Wang, L. Zhu, J. Fang, B. Xia, Z. Wang, K. Lu, W. Ma, Z. Wei, *Nature Comm.*, **2016**, *7*, 13740.

[49] L. Nian, K. Gao, Y. Jiang, Q. Rong, X. Hu, D. Yuan, F. Liu, X. Peng, T.P. Russell, G. Zhou, *Adv. Mater.*, **2017**, *29*, 1700616.

[50] S.D. Collins, N.A. Ran, M.C. Heiber, T.Q. Nguyen, *Adv. Energy Mater.*, **2017**, *7*, 1602242.

Supporting Information for

Self-Assembly of Chiral-at-End Diketopyrrolopyrroles : Symmetry Dependent Solution and Film Optical Activity and Photovoltaic Performance

By

Paul A. Hume, James P. Monks, Flavia Pop, E. Stephen Davies, Roderick C.I. MacKenzie and David B. Amabilino

Contents

1. Thin-Film Optical Absorption Measurements for Compounds 7-9

Thin-Film, Cast on Quartz Substrates

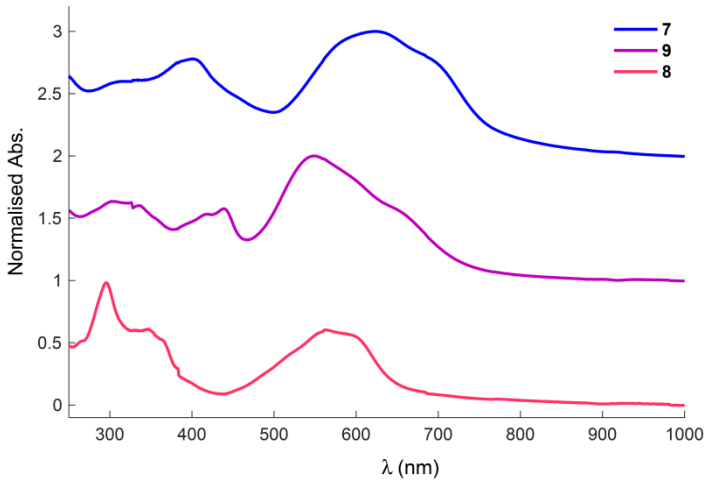

2. Cyclic Voltammograms for Compounds 7-9

Cyclic voltammograms of DPPs **7-9** in CH_2Cl_2 (2×10^{-4} M); scan rate 100 mV s^{-1}; supporting electrolyte tetrabutylammonium hexafluorophosphate (NBu_4PF_6, 0.4 M). Potentials are reported relative to the Fc^+/ Fc redox couple.

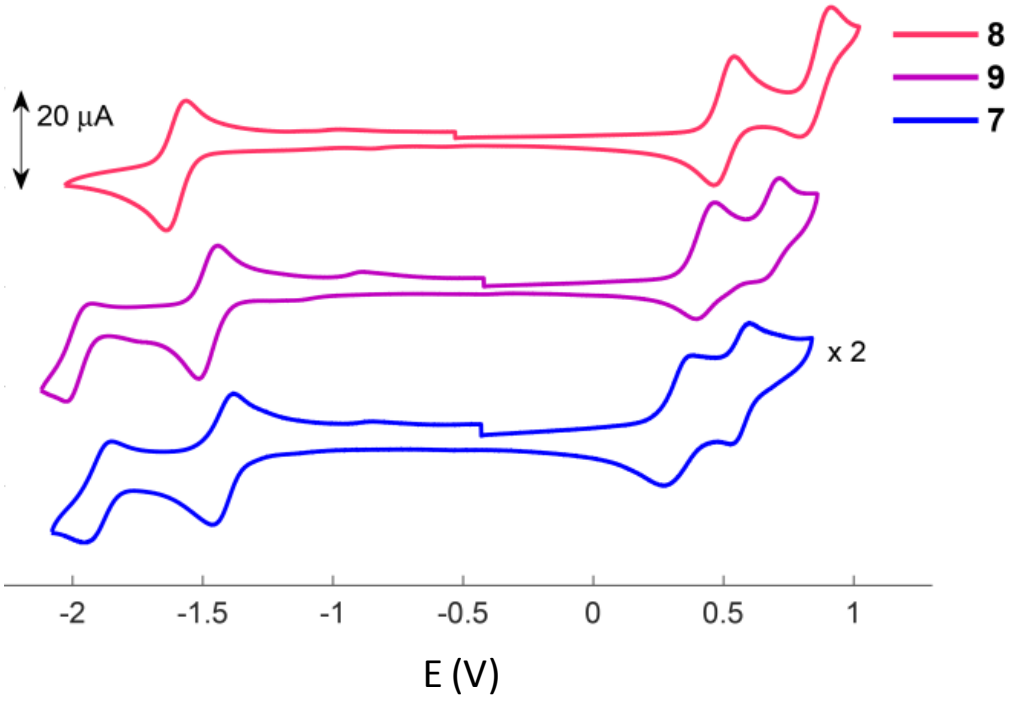

Reduced range cyclic voltammograms of DPPs **7** and **9** in CH_2Cl_2 (2×10^{-4} M); scan rate 100 mV s^{-1}; supporting electrolyte tetrabutylammonium hexafluorophosphate (NBu_4PF_6, 0.4 M). Potentials are reported relative to the Fc^+/ Fc redox couple.

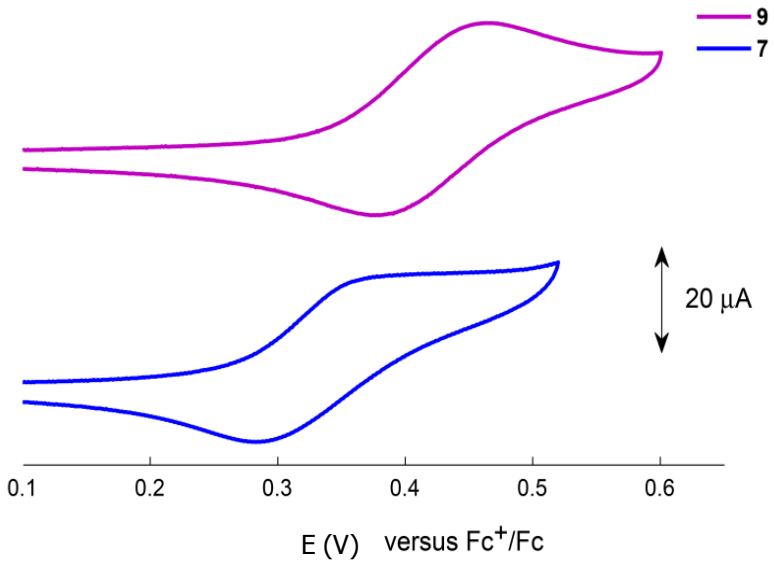

3. Theoretical Calculations

Quantum-chemical calculations were performed using the *Gaussian 03* software package.[2] In all cases, the normal modes associated with the optimised structures did not exhibit imaginary frequencies indicating that they represent minima on the potential energy surface.

3.1 Optimised Geometry of Compound 8, Energy and Orbital Contour Plots

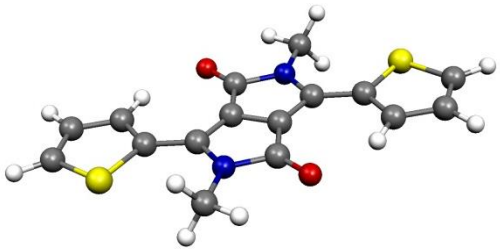

Optimised Geometry, $E = -1673.51593662$ Ha

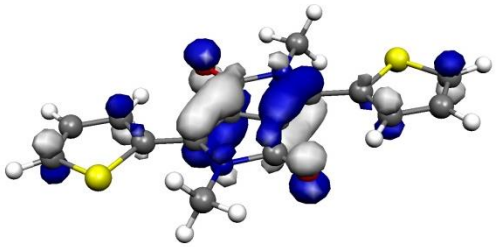

HOMO, $E = -5.185$ eV

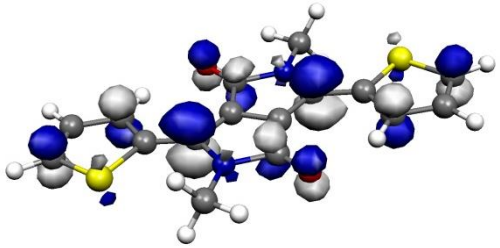

LUMO, $E = -2.720$ eV

3.2 Optimised Geometry of Compound 9, Energy and Orbital Contour Plots

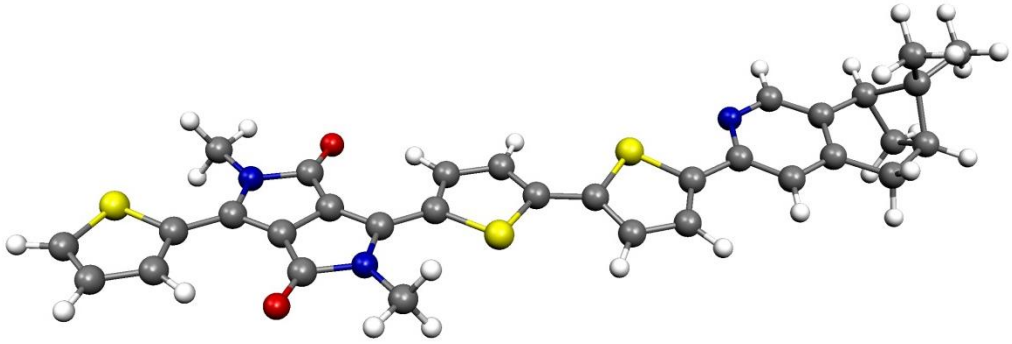

Optimised Geometry, $E = -2745.36692310$ Ha

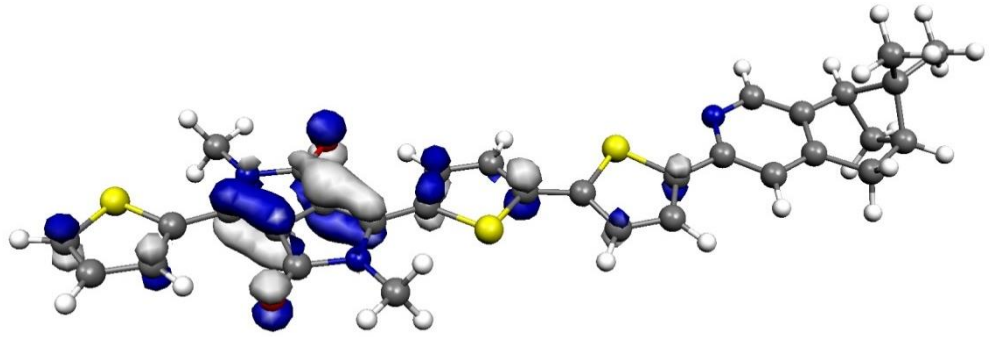

HOMO, E = −4.967 eV

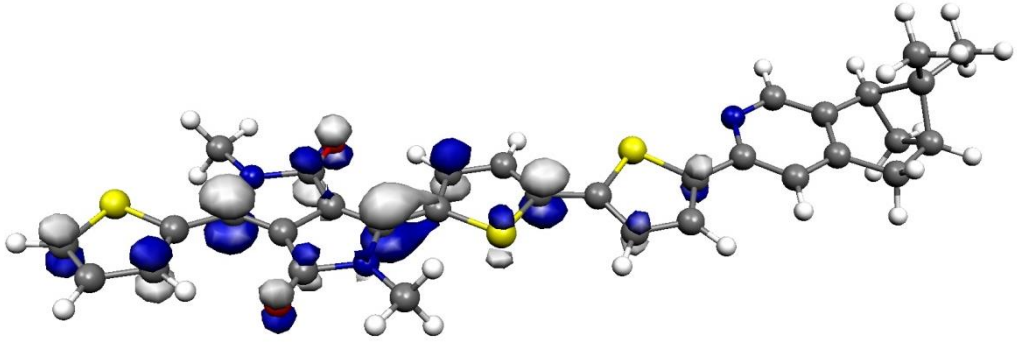

LUMO, E = −2.768 eV

3.3 Optimised Geometry of Compound 7, Energy and Orbital Contour Plots

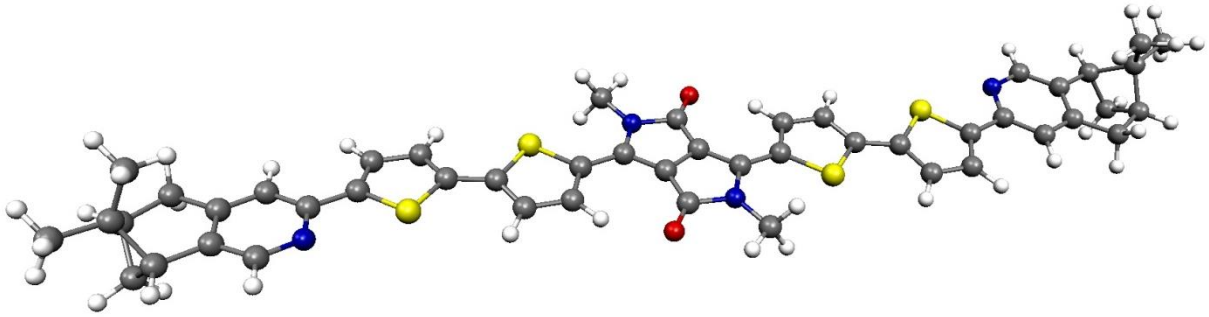

Optimised Geometry, E = −3817.21785866 Ha

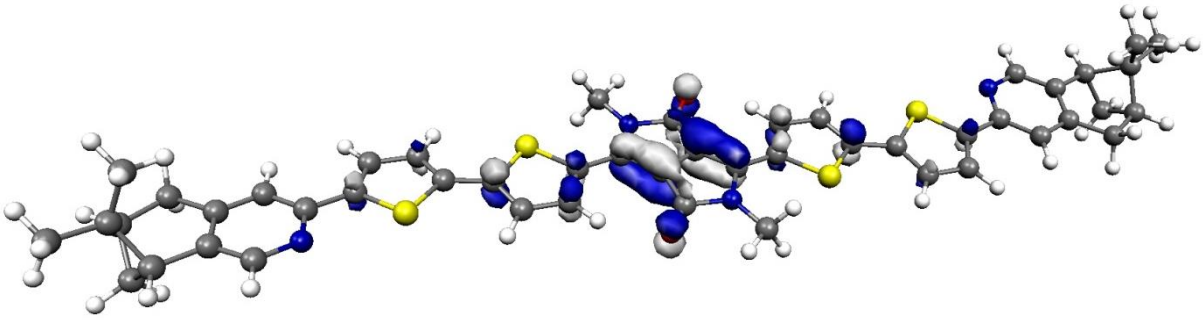

HOMO, E = −4.793 eV

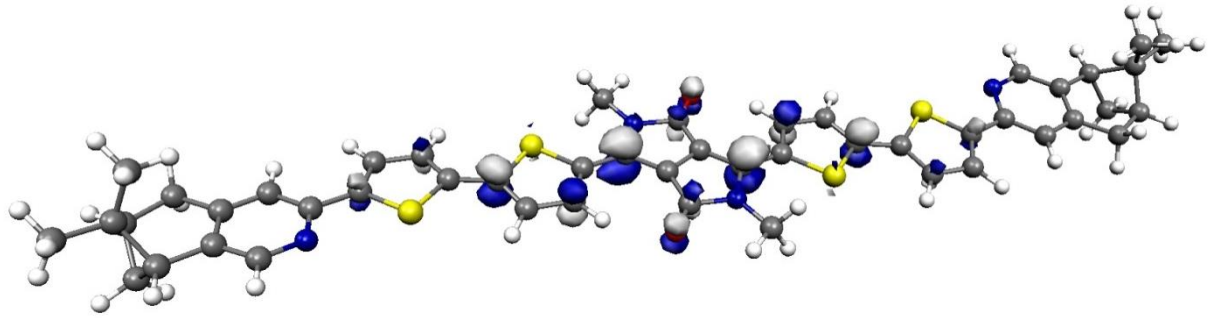

LUMO, E = −2.804 eV

3.4 Comparison of Experimental and Calculated Values

Experimental/ DFT

	E_{HOMO} (eV)[a]	E_{LUMO} (eV)[b]	E_g (eV)[c]	λ_{max} (nm, Expt.)	λ_{max} (nm, TD-DFT)
8	−5.32 /	−3.14 /	2.18 /	549, 509, 355, 340,	515, 318, 275
9	−5.20 /	−3.26 /	1.94 /	579, 413, 401, 316,	588, 413, 334,
7	−5.10 /	−3.29 /	1.81 /	647, 602, 421,[d]	664, 452, 407,

[a] The experimental value for the HOMO level was calculated from the potential at the onset of oxidation, using the vacuum level of Fc/ Fc^+ (4.8 eV) as reference.

[b] The experimental value for the LUMO level was calculated as the sum of the HOMO energy and the optical band-gap.

[c] The experimental value for the optical band-gap was calculated as 1240/ λ_{onset} (nm). Theoretical values are taken from the TD-DFT calculations.

[d] Appears as a shoulder on the absorption band centred at 381 nm.

4. Circular Dichroism of Compounds 7 and 9

CD Spectra of Compounds **7** and **9** as Molecularly Dissolved Solutions in THF

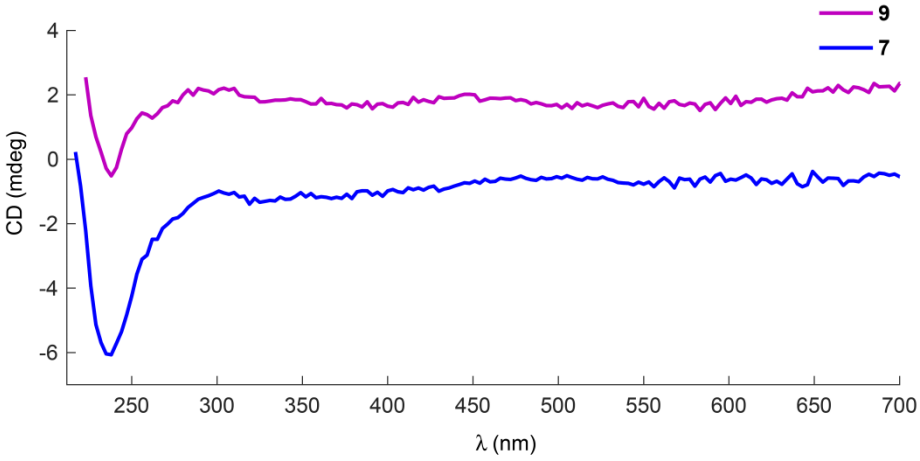

5. Device parameters of best performing cells for all conditions investigated

Materials	Blend Ratio (wt.)	Solvent	Spin Speed (rpm)	*Voc* (V)	*Jsc* (mA/cm^2)	FF (%)	Best Cell PCE
7:$PC_{61}BM$	1:1	$CHCl_3$	550	0.330	-0.0024	14	1.14e-4%
7:$PC_{61}BM$	1:1	$CHCl_3$	1000	0.0166	-0.491	26	0.00213 %
7:$PC_{61}BM$	1:1	$CHCl_3$	1000	0.210	-0.0266	21	0.00116 %
7:$PC_{61}BM$	1:1	$CHCl_3$	2000	0.100	-2.046	26	0.0539%
9:$PC_{61}BM$	1:1	PhCl	550	0.259	-0.201	27	0.0143%
9:$PC_{61}BM$	1:2	PhCl	500	0.195	-0.0293	20	0.0011%
9:$PC_{61}BM$	1:2	PhCl	800	0.193	-0.0786	19	0.0029%
9:$PC_{61}BM$	1:2	PhCl	1600	0.241	-0.212	20	0.0101%
9:$PC_{61}BM$	1:3	PhCl	500	0.218	-0.496	28	0.0304%
9:$PC_{61}BM$	1:3	PhCl	1000	0.158	-0.468	33	0.0267%
9:$PC_{61}BM$	1:3	PhCl	1500	0.175	-0.633	32	0.0359%
9:$PC_{61}BM$	1:3	PhCl	2000	0.218	-0.564	31	0.0377%
9:$P_{61}CBM$	1:3	PhCl	2500	0.204	-0.651	33	0.0438%
9:$PC_{61}BM$	1:5	PhCl	500	0.320	-0.451	21	0.0304%
9:$PC_{61}BM$	1:5	PhCl	1000	0.223	-0.307	21	0.0142%
9:$PC_{61}BM$	1:5	PhCl	1500	0.162	-0.163	23	0.0062%
9:$PC_{61}BM$	1:5	PhCl	2000	0.252	-0.236	17	0.0102%

6. Film thicknesses measured by AFM contouring in scratched samples[#]

9:PCBM 1:2

Measured thickness for PEDOT:PSS = 38.7167 nm

Spin rate (rpm)	Total layer thickness (active + PEDOT:PSS) (nm)	Approximate active layer thickness (nm)
550	85.4	46.7

9:PCBM 1:3

Spin rate (rpm)	Total layer thickness (active + PEDOT:PSS) (nm)	Approximate active layer thickness (nm)
500	83.3	44.6
1000	68.1	29.4
1500	62. 0	23.2
2000	60.3	21.6
2500	61.4	22.7

9:PCBM 1:5

Spin rate (rpm)	Total layer thickness (active + PEDOT:PSS) (nm)	Approximate active layer thickness (nm)
1000	55.0	16.3
1500	54.0	15.3
2000	47.1	47.1

[#] Each thickness value is derived from a mean of at least six profiles of scratches in the film.

7. References

1. R. R. Gagne, C. A. Koval and G. C. Lisensky, *Inorg. Chem.*, 1980, **19**, 2854.

2. Gaussian 03, Revision C.02, M. J. Frisch, G. W. Trucks, H. B. Schlegel, G. E. Scuseria, M. A. Robb, J. R. Cheeseman, J. A. Montgomery, Jr., T. Vreven, K. N. Kudin, J. C. Burant, J. M. Millam, S. S. Iyengar, J. Tomasi, V. Barone, B. Mennucci, M. Cossi, G. Scalmani, N. Rega, G. A. Petersson, H. Nakatsuji, M. Hada, M. Ehara, K. Toyota, R. Fukuda, J. Hasegawa, M. Ishida, T. Nakajima, Y. Honda, O. Kitao, H. Nakai, M. Klene, X. Li, J. E. Knox, H. P. Hratchian, J. B. Cross, V. Bakken, C. Adamo, J. Jaramillo, R. Gomperts, R. E. Stratmann, O. Yazyev, A. J. Austin, R. Cammi, C. Pomelli, J. W. Ochterski, P. Y. Ayala, K. Morokuma, G. A. Voth, P. Salvador, J. J. Dannenberg, V. G. Zakrzewski, S. Dapprich, A. D. Daniels, M. C. Strain, O. Farkas, D. K. Malick, A. D. Rabuck, K. Raghavachari, J. B. Foresman, J. V. Ortiz, Q. Cui, A. G. Baboul, S. Clifford, J. Cioslowski, B. B. Stefanov, G. Liu, A. Liashenko, P. Piskorz, I. Komaromi, R. L. Martin, D. J. Fox, T. Keith, M. A. Al-Laham, C. Y. Peng, A. Nanayakkara, M. Challacombe, P. M. W. Gill, B. Johnson, W. Chen, M. W. Wong, C. Gonzalez, and J. A. Pople, Gaussian, Inc., Wallingford CT, 2004.